On the treatment of anisotropic scattering in the heterogeneous variational nodal method

Wei Xiao, Tengfei Zhang *
School of Nuclear Science and Engineering, Shanghai Jiao Tong University, Shanghai 200240, China

Keywords : second-order transport equation, anisotropic scattering, variational nodal method, finite-element

1. Introduction

The variational nodal method (VNM) for solving the neutron equation was formulated based on a functional form of the neutron transport equation. VNM is compatible with various spatial and angular discretization schemes. It has been successfully applied in diverse homogenized problems[1]. Moreover, the heterogeneous VNM, which approximates the heterogeneous node using the finite element (FE) functions, shows great capacity in solving high-fidelity problems without spatial homogenizations[2]. The current high-fidelity calculation of heterogeneous VNM is implemented with the integral method, which cannot account for the anisotropic scattering sources. In the high-fidelity simulation of light water reactors and advanced reactors, the anisotropic scattering effect is of importance. However, the procedure to formulate the VNM with anisotropic sources differs notably from the isotropic case due to presence of the odd-parity terms in the second-order transport equation[3][4]. Therefore, to perform high-fidelity calculations more accurately, the anisotropic formulation of heterogeneous VNM is required.

VITAS is a multi-purpose neutron transport solver developed at the Shanghai Jiao Tong University for solving steady and time-dependent neutron transport problems based on the VNM[5]. It is compatible with various geometries, including the geometry made up with heterogeneous nodes with FE subdivisions. However, the latest version of VITAS can only deal with isotropic problems. In this paper, the heterogeneous VNM with discrete ordinates (S_N) method is formulated in the anisotropic problem. Subsequently, the anisotropic solver is developed based on the VITAS and verified against an anisotropic slab problem.

2. Methods

In the VNM, by defining the even- and odd-parity fluxes ψ^+ and ψ^-, we add and subtract transport equation evaluated at $\mathbf{\Omega}$ and $-\mathbf{\Omega}$ to obtain[1][6]

$$\mathbf{\Omega}\cdot\nabla\psi_g^-(\mathbf{r},\mathbf{\Omega})+\Sigma_{tg}(\mathbf{r})\psi_g^+(\mathbf{r},\mathbf{\Omega})=q_g^+(\mathbf{r},\mathbf{\Omega}) \quad (1)$$

$$\mathbf{\Omega}\cdot\nabla\psi_g^+(\mathbf{r},\mathbf{\Omega})+\Sigma_{tg}(\mathbf{r})\psi_g^-(\mathbf{r},\mathbf{\Omega})=q_g^-(\mathbf{r},\mathbf{\Omega}) \quad (2)$$

where g denotes the energy group, Σ_{tg} is the total cross-section, q is the source term, $\mathbf{\Omega}$ represents the direction, and $\mathbf{r}$ represents the position containing (x,y,z) in the Cartesian coordinate. Eliminating the explicit expression of ψ^- between Eqs. (1) and (2) yields the even- and odd-parity equations

$$\begin{aligned}\Sigma_{tg}(\mathbf{r})\psi_g^+(\mathbf{r},\mathbf{\Omega})-\mathbf{\Omega}\cdot\nabla\Sigma_{tg}^{-1}(\mathbf{r})\mathbf{\Omega}\cdot\nabla\psi_g^+(\mathbf{r},\mathbf{\Omega})\\ =q_g^+(\mathbf{r},\mathbf{\Omega})-\mathbf{\Omega}\cdot\nabla\Sigma_{tg}^{-1}(\mathbf{r})q_g^-(\mathbf{r},\mathbf{\Omega})\end{aligned} \quad (3)$$

$$\begin{aligned}\psi_g^-(\mathbf{r},\mathbf{\Omega})=-\Sigma_{tg}^{-1}(\mathbf{r})\mathbf{\Omega}\cdot\nabla\psi_g^+(\mathbf{r},\mathbf{\Omega})\\ +\Sigma_{tg}^{-1}(\mathbf{r})q_g^-(\mathbf{r},\mathbf{\Omega})\end{aligned} \quad (4)$$

Assuming there is no external source in the system, and considering the anisotropy of the scattering source, the time-independent even- and odd parity source terms q^+ and q^- are

$$\begin{aligned}q_g^+(\mathbf{r},\mathbf{\Omega})=\frac{\chi_g}{k_{\text{eff}}}\sum_{g'}\nu\Sigma_{fg'}(\mathbf{r})\phi_{g'}(\mathbf{r})\\ +\sum_{g'}\int d\mathbf{\Omega}'\Sigma_{sg'g}^+(\mathbf{r},\mathbf{\Omega}'\cdot\mathbf{\Omega})\psi_g^+(\mathbf{r},\mathbf{\Omega}')\end{aligned} \quad (5)$$

$$q_g^-(\mathbf{r},\mathbf{\Omega})=\sum_{g'}\int d\mathbf{\Omega}'\Sigma_{sg'g}^-(\mathbf{r},\mathbf{\Omega}'\cdot\mathbf{\Omega})\psi_g^-(\mathbf{r},\mathbf{\Omega}') \quad (6)$$

where k_{eff} is the eigenvalue, χ is the prompt fission spectrum, $\nu\Sigma_f$ is the nu-fission cross-section, Σ_s^+ and Σ_s^- are even and odd scattering cross-sections respectively, and the scalar flux is given by

$$\phi_g(\mathbf{r})=\int d\mathbf{\Omega}'\psi_g^+(\mathbf{r},\mathbf{\Omega}') \quad (7)$$

The even- and odd scattering cross-sections are expanded with even- and odd-terms of Legendre polynomials[4], respectively

$$\Sigma_{sg'g}^+(\mathbf{r},\mathbf{\Omega}'\cdot\mathbf{\Omega})=\sum_{l=0,2,4,...}(2l+1)\Sigma_{sg'g,l}(\mathbf{r})P_l(\mathbf{\Omega}'\cdot\mathbf{\Omega}) \quad (8)$$

$$\Sigma_{sg'g}^-(\mathbf{r},\mathbf{\Omega}'\cdot\mathbf{\Omega})=\sum_{l=1,3,5,...}(2l+1)\Sigma_{sg'g,l}(\mathbf{r})P_l(\mathbf{\Omega}'\cdot\mathbf{\Omega}) \quad (9)$$

l is the order of Legendre polynomials.

2.1 Variational formulation of even-parity equation

The functional of Eq. (3) for node ν with the interface Γ, can be written as

$$\begin{aligned}F_\nu=\int_\nu dV\int d\Omega\left\{\begin{array}{l}\Sigma_{tg}^{-1}(\mathbf{r})\left[\mathbf{\Omega}\cdot\nabla\psi_g^+(\mathbf{r},\mathbf{\Omega})\right]^2\\+\Sigma_{tg}\psi_g^{+2}(\mathbf{r},\mathbf{\Omega})\end{array}\right\}\\ -2\int_\nu dV\int d\Omega\psi_g^+(\mathbf{r},\mathbf{\Omega})q_g^+(\mathbf{r},\mathbf{\Omega})\\ -2\int_\nu dV\int d\Omega\Sigma_{tg}^{-1}(\mathbf{r})\mathbf{\Omega}\cdot\nabla\psi_g^+(\mathbf{r},\mathbf{\Omega})q_g^-(\mathbf{r},\mathbf{\Omega})\\ +2\int_\Gamma d\Gamma\int d\Omega\mathbf{\Omega}\cdot\mathbf{n}\psi_g^+(\mathbf{r},\mathbf{\Omega})\psi_g^-(\mathbf{r},\mathbf{\Omega})\end{aligned} \quad (10)$$

In the S_N method, the angular flux is solved for a set of direction $\mathbf{\Omega}_n, n=1,...,N$ on the unit sphere, and weights w_n are assigned to each direction. In this code, the directions are chosen based on Legendre-Chebychev quadrature. In the heterogeneous VNM, the radial term of the flux is approximated with FE basis functions, while the axial term is expanded with orthogonal polynomials. Within the node v and direction $\mathbf{\Omega}_n$, the spatial distribution of the even-parity flux is approximated by

$$\psi^+(\mathbf{r},\mathbf{\Omega}_n) \approx \underline{f}_z^T(z)\otimes \underline{g}^T(x,y)\underline{\psi}_n^+ \tag{11}$$

and the scalar flux can be expanded as

$$\begin{aligned}\phi(\mathbf{r}) &\approx \underline{f}_z^T(z)\otimes \underline{g}^T(x,y)\sum_n w_n \underline{\psi}_n^+ \\ &= \underline{f}_z^T(z)\otimes \underline{g}^T(x,y)\underline{\phi}\end{aligned} \tag{12}$$

where $f_z(z)$ is a vector of orthogonal polynomials defined at node v and $g(x,y)$ is a vector of continuous FE basis functions. Triangular and quadrilateral iso-parametric quadratic FEs were employed to map the curved interfaces between materials. Fig. 1 shows a FE mesh with 32 elements, used for describing a fuel pin cell.

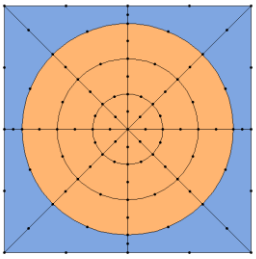

Fig. 1 A FE mesh for a fuel pin

To not confuse the nodal and interfacial odd-parity flux, the interfacial odd-parity is represented with ξ in the following. The interfacial odd-parity flux at the lateral interface Γ_γ is approximated as

$$\xi_\gamma(\mathbf{\Omega}_n) \approx \underline{f}_\gamma^T(\zeta)\underline{\xi}_{n,\gamma} \quad \gamma=\pm x,\pm y \quad \zeta = y,x \tag{13}$$

and at the axial interfaces, the odd-parity flux as approximated as

$$\xi_z(\mathbf{\Omega}_n) \approx \underline{h}^T(x,y)\underline{\xi}_{n,z} \tag{14}$$

where f_γ are polynomials defined on the lateral surfaces and $h(x,y)$ denotes a vector of piecewise constants.

Inserting the trial functions into Eqs. (11), (13) and (14) yields the following discretized functional

$$\begin{aligned}F_{vn}\left[\psi^+,\chi\right] &= \underline{\psi}_{gn}^{+T}\underline{\underline{A}}_{gn}\underline{\psi}_{gn}^+ - 2\underline{\psi}_{gn}^{+T}\underline{q}_{gn}^+ \\ &-2\underline{\psi}_{gn}^{+T}\underline{q}_{gn}^- + 2\underline{\psi}_{gn}^{+T}\underline{\underline{D}}\underline{\xi}_{gn}'\end{aligned} \tag{15}$$

where the coefficient matrices are defined in Table 1.

Table 1 Coefficient matrices of the even-parity equations

$$\begin{aligned}
\underline{\underline{A}}_{gn} &= \underline{\underline{I}}_z \otimes \sum_{i,j=x,y}\Omega_{n,i}\Omega_{n,j}\underline{\underline{P}}_{g,ij} + \Omega_{n,z}^2\underline{\underline{P}}_{zz}\otimes\underline{\underline{F}}_{g-} \\
&\quad + \underline{\underline{I}}_z\otimes\underline{\underline{F}}_{gt} + \sum_{i=x,y}\Omega_{n,i}\Omega_{n,z}\left(\underline{\underline{P}}_z^T\otimes\underline{\underline{P}}_{g,i} + \underline{\underline{P}}_z\otimes\underline{\underline{P}}_{g,i}^T\right) \\
\underline{\underline{D}} &= \left[\underline{\underline{D}}_{+x},\underline{\underline{D}}_{-x},...,\underline{\underline{D}}_{-z}\right] \\
\underline{\underline{D}}_\gamma &= \Delta z\int_{\Gamma_\gamma} d\zeta\, \underline{g}(x,y)|_\gamma\, \underline{f}_\gamma^T(\zeta) \quad \gamma=\pm x,\pm y \quad \zeta=y,x \\
\underline{\underline{D}}_z &= \int dxdy\,\underline{g}(x,y)\underline{h}^T(x,y) \\
\underline{\underline{P}}_{g,ij} &= \Delta z\int dxdy\,\Sigma_{tg}^{-1}(x,y)\nabla_i\underline{g}(x,y)\nabla_j\underline{g}^T(x,y) \\
\underline{\underline{P}}_{zz} &= \int dz\,\nabla_z\underline{f}_z(z)\nabla_z\underline{f}_z^T(z) \\
\underline{\underline{F}}_{g-} &= \int dxdy\,\Sigma_{tg}^{-1}(x,y)\underline{g}^T(x,y)\underline{g}(x,y) \\
\underline{\underline{F}}_{gt} &= \Delta z\int dxdy\,\Sigma_{tg}(x,y)\underline{g}^T(x,y)\underline{g}(x,y) \\
\underline{\underline{P}}_z &= \int dz\,\nabla_z\underline{f}_z(z)\underline{f}_z^T(z) \\
\underline{\underline{P}}_{g,i} &= \int dxdy\,\Sigma_{tg}^{-1}(x,y)\nabla_i\underline{g}(x,y)\underline{g}^T(x,y)
\end{aligned}$$

The surficial odd-parity moments and source moments vector are defined as

$$\underline{\xi}_{gn}'^T = \left[\Omega_{n,x}\underline{\xi}_{gn,+x}^T, \Omega_{n,-x}\underline{\xi}_{gn,-x}^T,...,\Omega_{n,-z}\underline{\xi}_{gn,-z}^T\right] \tag{16}$$

$$\underline{q}_{gn}^+ = \int_v dV\underline{f}_z(z)\otimes\underline{g}(x,y)q_{gn}^+(\mathbf{r}) \tag{17}$$

$$\begin{aligned}\underline{q}_{gn}^- &= \int dV\Sigma_{tg}^{-1}(\mathbf{r})\Omega_{n,z}\nabla_z\underline{f}_z(z)\otimes\underline{g}(x,y)q_{gn}^-(\mathbf{r}) \\ &+\sum_{i=x,y}\int dV\Sigma_{tg}^{-1}(\mathbf{r})\Omega_{n,i}\underline{f}_z(z)\otimes\nabla_i\underline{g}(x,y)q_{gn}^-(\mathbf{r})\end{aligned} \tag{18}$$

The definitions of all matrices in the even-parity equation were detailed in a previous study[6]. Requiring the discretized functional in Eq. (15) to be stationary with respect to variations in ψ^+ yields the discretized even-parity equation as

$$\underline{\underline{A}}_{gn}\underline{\psi}_{gn}^+ = \underline{q}_{gn}^+ + \underline{q}_{gn}^- - \underline{\underline{D}}\underline{\xi}_{gn}' \tag{19}$$

Similarly, the nodal odd-parity flux is approximated as

$$\psi^-(\mathbf{r},\mathbf{\Omega}_n) \approx \underline{f}_z^T(z)\otimes\underline{g}^T(x,y)\underline{\psi}_n^- \tag{20}$$

Choosing the expansion function as the trial function, the discretized weak form of the odd-parity equation is obtained as

$$\underline{\underline{F}}\underline{\psi}_{gn}^- = -\underline{\underline{P}}_{gn}\underline{\psi}_{gn}^+ + \underline{q}_{gn}^{-'} \tag{21}$$

where the source moments are defined as

$$\underline{q}_{gn}^{-'} = \int dV\Sigma_{tg}^{-1}(\mathbf{r})\underline{f}_z(z)\otimes\underline{g}(x,y)q_{gn}^-(\mathbf{r}) \tag{22}$$

and the coefficient matrices are defined in Table 2.

Table 2 Coefficient matrices of the odd-parity equations

$$\underline{\underline{F}} = \underline{\underline{I}}_z \otimes \int dxdy\, \underline{g}^T(x,y)\,\underline{g}(x,y)$$
$$\underline{\underline{P}}_{gn} = \sum_{i=x,y} \Omega_{n,i}\, \underline{\underline{I}}_z \otimes \underline{\underline{P}}^T_{g,i} + \Omega_{n,z}\, \underline{\underline{P}}^T_z \otimes \underline{\underline{F}}_{g-}$$

2.2 Flat source treatment

In the traditional FE method, the number of unknowns is equal to the degree of freedoms of the FE mesh, which will incur significant computational cost and memory usage when high-order iso-parametric FEs are applied. To alleviate this burden, the flat source approximation is applied, and the element-wise flux are stored. For example, the moments of element-wise average even-parity flux are defined as

$$\begin{aligned}\overline{\underline{\psi}}^+ &= \int dV \underline{f}_z(z) \otimes \underline{h}^T(x,y)\, \underline{f}_z^T(z) \otimes \underline{g}^T(x,y)\, \underline{\psi}^+ \\ &= \left(\underline{\underline{I}}_z \otimes \underline{\underline{\Xi}}^{-1} \underline{\underline{D}}_z^T\right) \underline{\psi}^+\end{aligned} \tag{23}$$

where $\underline{\underline{\Xi}}$ is diagonal matrix composed of the element areas. With the element-wise moments, the flat even-parity source is defined as

$$q^+_{gn}(\mathbf{r}) = \underline{f}_z^T(z) \otimes \underline{h}^T(x,y)\, \overline{\underline{q}}^+_{gn} \tag{24}$$

where the flat source moments in Eq. (24) are obtained as

$$\begin{aligned}\overline{\underline{q}}^+_{gn} &= \sum_{g'} \sum_{n'} w_{n'} \underline{\underline{\Sigma}}_{sg'g} \left(\mathbf{\Omega}_n \cdot \mathbf{\Omega}_{n'}\right) \overline{\underline{\psi}}^+_{g'n'} \\ &+ \frac{\underline{\underline{\chi}}_g}{k_{\text{eff}}} \sum_{g'} \nu \underline{\underline{\Sigma}}_{fg'} \overline{\underline{\phi}}_g\end{aligned} \tag{25}$$

Then, the source moments $\underline{q}^+_{gn}$ is obtained by inserting Eq. (24) into Eq. (17)

$$\underline{q}^+_{gn} = \underline{\underline{I}}_z \otimes \underline{\underline{D}}_z\, \overline{\underline{q}}^+_{gn} \tag{26}$$

Similarly, the odd-parity source moments in Eqs. (18) and (22) are given by

$$\underline{q}^-_{gn} = \underline{\underline{H}}^-_{gn}\, \overline{\underline{q}}^-_{gn} \tag{27}$$

$$\underline{q}^{-'}_{gn} = \underline{\underline{I}}_z \otimes \underline{\underline{D}}_{g-}\, \overline{\underline{q}}^-_{gn} \tag{28}$$

where

$$\underline{\underline{H}}^-_{gn} = \sum_{i=x,y} \Omega_{n,i}\, \underline{\underline{I}}_z \otimes \underline{\underline{D}}_{g,i} + \Omega_{n,z}\, \underline{\underline{P}}_z \otimes \underline{\underline{D}}_{g-} \tag{29}$$

$$\underline{\underline{D}}_{g,i} = \int dxdy\, \Sigma^{-1}_{tg}(x,y)\, \nabla_i \underline{g}(x,y)\, \underline{h}^T(x,y) \tag{30}$$

$$\underline{\underline{D}}_{g-} = \int dxdy\, \Sigma^{-1}_{tg}(x,y)\, \underline{g}(x,y)\, \underline{h}^T(x,y) \tag{31}$$

2.3 Nodal response matrix equations

By requiring the projection of nodal even-parity flux to be continuous across the interfaces and defining the partial currents j^+ and j^- [6], the nodal response matrix equations are derived from Eqs. (19) and (21) as

$$\underline{j}^+_{gn} = \underline{\underline{B}}^+_{gn}\, \overline{\underline{q}}^+_{gn} + \underline{\underline{B}}^-_{gn}\, \overline{\underline{q}}^-_{gn} + \underline{\underline{R}}^+_{gn}\, \underline{j}^-_{gn} \tag{32}$$

$$\overline{\underline{\psi}}^+_{gn} = \underline{\underline{V}}^+_{gn}\, \overline{\underline{q}}^+_{gn} + \underline{\underline{V}}^-_{gn}\, \overline{\underline{q}}^-_{gn} - \underline{\underline{C}}^+_{gn} \left(\underline{j}^+_{gn} - \underline{j}^-_{gn}\right) \tag{33}$$

$$\overline{\underline{\psi}}^-_{gn} = \underline{\underline{K}}^+_{gn}\, \overline{\underline{q}}^+_{gn} + \underline{\underline{K}}^-_{gn}\, \overline{\underline{q}}^-_{gn} - \underline{\underline{C}}^-_{gn} \left(\underline{j}^+_{gn} - \underline{j}^-_{gn}\right) \tag{34}$$

The relevant matrices are defined in Table 3.

Table 3 Response matrices

$$\underline{\underline{B}}^+_{gn} = \frac{1}{2}\left(\frac{1}{2}\underline{\underline{G}}_{gn} + \underline{\underline{I}}\right)^{-1} \underline{\underline{U}}_{gn}\, \underline{\underline{I}}_z \otimes \underline{\underline{D}}_z$$
$$\underline{\underline{B}}^-_{gn} = \frac{1}{2}\left(\frac{1}{2}\underline{\underline{G}}_{gn} + \underline{\underline{I}}\right)^{-1} \underline{\underline{U}}_{gn}\, \underline{\underline{H}}^-_{gn}$$
$$\underline{\underline{G}}_{gn} = \underline{\underline{D}}^T \underline{\underline{A}}^{-1}_{gn} \underline{\underline{D}}$$
$$\underline{\underline{U}}_{gn} = \underline{\underline{A}}^{-1}_{gn} \underline{\underline{D}}$$
$$\underline{\underline{V}}^+_{gn} = \underline{\underline{I}}_z \otimes \underline{\underline{\Xi}}^{-1} \underline{\underline{D}}^T_z \underline{\underline{A}}^{-1}_{gn} \underline{\underline{I}}_z \otimes \underline{\underline{D}}_z$$
$$\underline{\underline{V}}^-_{gn} = \underline{\underline{I}}_z \otimes \underline{\underline{\Xi}}^{-1} \underline{\underline{D}}^T_z \underline{\underline{A}}^{-1}_{gn} \underline{\underline{H}}^-_{gn}$$
$$\underline{\underline{C}}^+_{gn} = \underline{\underline{I}}_z \otimes \underline{\underline{\Xi}}^{-1} \underline{\underline{D}}^T_z \underline{\underline{A}}^{-1}_{gn} \underline{\underline{D}}$$
$$\underline{\underline{K}}^+_{gn} = -\underline{\underline{I}}_z \otimes \underline{\underline{\Xi}}^{-1} \underline{\underline{D}}^T_z \underline{\underline{F}}^{-1} \underline{\underline{P}}_{gn} \underline{\underline{A}}^{-1}_{gn} \underline{\underline{I}}_z \otimes \underline{\underline{D}}_z$$
$$\underline{\underline{K}}^-_{gn} = \underline{\underline{I}}_z \otimes \underline{\underline{\Xi}}^{-1} \underline{\underline{D}}^T_z \underline{\underline{F}}^{-1} \left(\underline{\underline{I}}_z \otimes \underline{\underline{D}}_{g-} - \underline{\underline{P}}_{gn} \underline{\underline{A}}^{-1}_{gn} \underline{\underline{H}}^-_{gn}\right)$$
$$\underline{\underline{C}}^-_{gn} = -\underline{\underline{I}}_z \otimes \underline{\underline{\Xi}}^{-1} \underline{\underline{D}}^T_z \underline{\underline{F}}^{-1} \underline{\underline{P}}_{gn} \underline{\underline{A}}^{-1}_{gn} \underline{\underline{D}}$$

3. Results

3.1 One-group slab problem

The preliminary test problem is an anisotropic eigenvalue problem in one-dimensional slab geometry. This problem contains two regions, which are shown in Fig. 2. The cross-sections are listed in Table 4 with scattering order up to P_3.

In the heterogeneous VNM calculation, the regions are discretized into 20 nodes expanded with second-order polynomials, and the height of each node is 0.25 cm. A quadrature of S_{36} is applied, which contains 361 quadrature points on the hemisphere. The polar angle ϕ defined in the calculation is also illustrated in Fig. 2. The reference solution is generated using the multi-group mode of OpenMC[7].

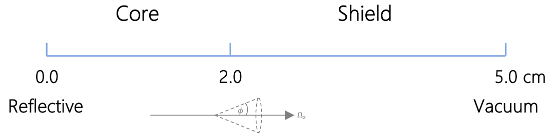

Fig. 2 Layout of the one-group slab problem

Table 4 Cross-sections of one-group slab problem (unit: cm^{-1})

Region	Σ_t	$\nu\Sigma_f$	Σ_{s0}	Σ_{sl} $l=1,2,3$
Core	1.10	1.0	0.60	0.10
Shield	0.95	0.0	0.55	0.15

The eigenvalues k_{eff} are compared in Table 5. The results indicate that the changes of eigenvalues in the VNM by increasing the scattering order are highly consistent with those in the OpenMC. When the scattering order is P_1, Δk_{eff} in OpenMC and VNM are -2177 and -2216 pcm, respectively. As the scattering order increases to P_2, Δk_{eff} are -1931 and -1982 pcm, respectively.

Table 5 k_{eff} in the one-group slab problem

P_l	k_{eff} * (MC)	k_{eff} (VNM)	Δk_{eff} ** (MC)	Δk_{eff} (VNM)
P_0	1.69823	1.69925	0	0
P_1	1.67646	1.67709	-2177	-2216
P_2	1.67898	1.67994	-1925	-1931
P_3	1.67892	1.67943	-1931	-1982

* The std. of k_{eff} in MC is ~15 pcm

** Δk_{eff} is the difference of k_{eff} with P_l and P_0 scattering (unit: pcm)

Fig. 3 illustrates the spatial distribution of scalar flux. It shows that in the core region, the scattering order has an insignificant effect on the scalar flux. However, in the shield region, the P_0 scattering underestimates the flux significantly with relative differences up to 30.0%.

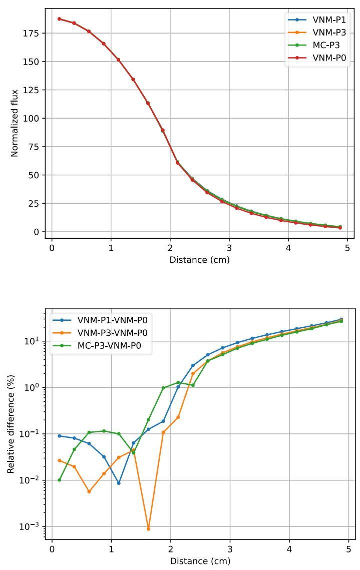

Fig. 3 Comparison of spatial distribution of scalar flux with different scattering orders

Fig. 4 compares polar distributions of angular flux, even- and odd-parity flux with P_0 and P_3 scattering, at node-1 (0.0-0.25 cm), -8 (1.75-2.00 cm) and -20 (4.75-5.00 cm). At the node-1, the angular flux shows symmetry with respect to $\phi = 90^{\circ}$ since the node is near the reflective boundary. At the node-8, which locates near the interface of the core and field, the even-parity flux shows great isotropy. However, contributed by the extremely anisotropic odd-parity flux, which is induced by the large gradient near the interface, the angular flux is in highly anisotropic.

At the node-20, which is locates at the vacuum boundary, the angular flux with P_0 scattering deviates significantly from that with P_3 scattering. It can be found when P_0 scattering is implemented, the angular flux on $\phi \sim \left(0^{\circ}, 90^{\circ}\right)$, which is the outgoing direction with respect to the boundary, is much smaller due to underestimation of both even- and odd-parity flux. The underestimation of the outgoing angular flux results in the smaller leakage and thus larger eigenvalue.

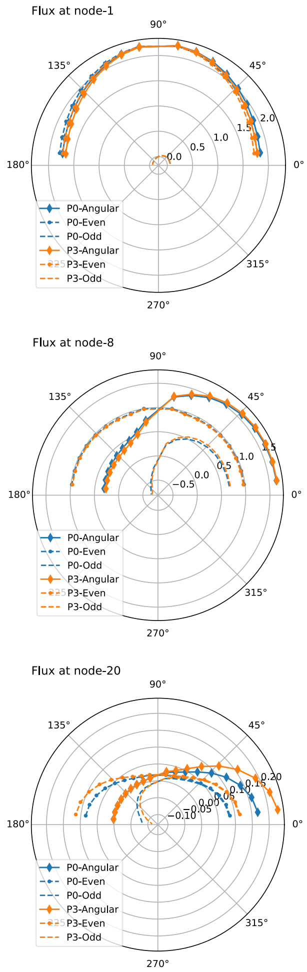

Fig. 4 Comparison of polar distribution of flux at different locations

4. Conclusions

This work demonstrates the formulation of the S_N-heterogeneous VNM in the anisotropic problem. The anisotropic heterogeneous VNM solver is developed based on the VITAS. The solver enables solving anisotropic transport equation and the analysis to both even- and odd-parity flux. An anisotropic slab problem is used to preliminarily verify the solver. The results in the test problem are in consistency with the reference solutions from the multi-group OpenMC. The analysis to the angular dependence of the flux also illustrates the effects due to the scattering order. Future efforts will focus on applying the anisotropic heterogeneous VNM on the high-fidelity calculations of advanced reactors. Moreover, the anisotropic solver will be applied to formulate consistent transient solver based on the second-order transport equation.

REFERENCES

[1] Zhang, T., & Li, Z. (2022). Variational nodal methods for neutron transport: 40 years in review. Nuclear Engineering and Technology, 54(9), 3181-3204.
[2] Zhang, T., Lewis, E. E., Smith, M. A., Yang, W. S., & Wu, H. (2017). A Variational Nodal Approach to 2D/1D Pin Resolved Neutron Transport for Pressurized Water Reactors. Nuclear Science and Engineering, 186(2), 120-133.
[3] Shemon, E. R., Smith, M. A., & Lee, C. H.. PROTEUS-SN Methodology Manual. United States.
[4] Palmiotti, G., Carrico, C. B., & Lewis, E. E. (1993). Variational Nodal Transport Methods with Anisotropic Scattering. Nuclear Science and Engineering, 115(3), 233-243.
[5] Zhang, T., Xiao, W., Yin, H., Sun, Q., & Liu, X. (2022). VITAS: A multi-purpose simulation code for the solution of neutron transport problems based on variational nodal methods. Annals of Nuclear Energy, 178, 109335.
[6] Zhang, T., Wang, Y., Lewis, E. E., Smith, M. A., Yang, W. S., & Wu, H. (2017). A Three-Dimensional Variational Nodal Method for Pin-Resolved Neutron Transport Analysis of Pressurized Water Reactors. Nuclear Science and Engineering, 188(2), 160-174.
[7] Romano, P. K., Horelik, N. E., Herman, B. R., Nelson, A. G., Forget, B., & Smith, K. (2015). OpenMC: A state-of-the-art Monte Carlo code for research and development. Annals of Nuclear Energy, 82, 90-97.